FUNDAMENTALS OF CAVITATION

edited by

Jean-Pierre FRANC
Jean-Marie MICHEL

Grenoble Sciences
2003

Grenoble Sciences

"Grenoble Sciences", directed by Prof. Jean Bornarel, was created ten years ago by the Joseph Fourier University of Grenoble, France (Science, Technology and Medecine) to select and publish original projects. Anonymous referees choose the best projects and then a Reading Committee interacts with the authors as long as necessary to improve the quality of the manuscripts.

(Contact: Tel: (33) 4 76 51 46 95 - E-mail: Grenoble.Sciences@ujf-grenoble.fr)

The "Fundamentals of Cavitation" Reading Committee included the following members:

- **Professeur Hiroharu Kato**, Faculty of Engineering, Tokyo University, Japan
- **Professeur Kirill V. Rozhdestvensky**, Saint-Petersburg State Marine Technical University, Russia
- **Professeur Dr.-Ing. Bernd Stoffel**, Darmstadt University of Technology, Germany

Front Cover Photo:
Photograph Bassin d’Essais des Carènes, Délégation Générale à l’Armement (DGA), Val de Reuil, France.

EXTRAITS

to a reduction in local pressure, possibly to a value below the vapor pressure of the liquid, thus producing vapor. A similar phenomenon can be found in volumetric pumps for fuel injection in engines. Head losses and rapid acceleration of the liquid column can result in low pressures, causing cavitation and consequent partial filling of the chamber.

1.1.2. VAPOR PRESSURE

The concept of vapor pressure is best considered from the viewpoint of classical thermodynamics. In the phase diagram for, say, water (fig. 1.1), the curve from the triple point T_r to the critical point C separates the liquid and vapor domains. Crossing that curve is representative of a reversible transformation under static (or equilibrium) conditions, i.e. evaporation or condensation of the fluid at pressure p_v, known as the vapor pressure. This is a function of the temperature T.

Following from this, cavitation in a liquid can be made occur by lowering the pressure at an approximately constant temperature, as often happens locally in real flows. Cavitation thus appears similar to boiling, except that the driving mechanism is not a temperature change but a pressure change, generally controlled by the flow dynamics.

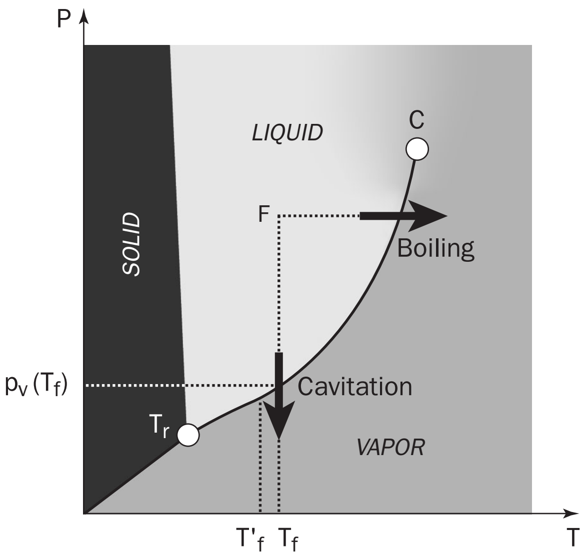

1.1
Phase diagram

In most cases (with cold water, in particular), only a relatively small amount of heat is required for the formation of a significant volume of vapor. The surrounding liquid (the heat source for vaporization) therefore shows only a very minor temperature change. The path in the phase diagram is practically isothermal (see fig. 1.1).

However, in some cases, the heat transfer needed for the vaporization is such that phase change occurs at a temperature T' lower than the ambient liquid temperature T. The temperature difference $T - T'$ is called thermal delay in cavitation.

It is greater when the ambient temperature is closer to the critical temperature of the fluid. This phenomenon may become important e.g. when pumping cryogenic liquids in rocket engines. It will be considered in chapters 5 and 8.

From a purely theoretical point of view, several steps can be distinguished during the first instants of cavitation:

- breakdown or void creation,
- filling of this void with vapor, and
- eventual saturation with vapor.

In reality, those phases are effectively simultaneous with the second step being so rapid that instantaneous saturation of the void with vapor can be justifiably assumed.

It must be kept in mind that the curve $p_v(T)$ is not an absolute boundary between liquid and vapor states. Deviations from this curve can exist in the case of rapid phase change.

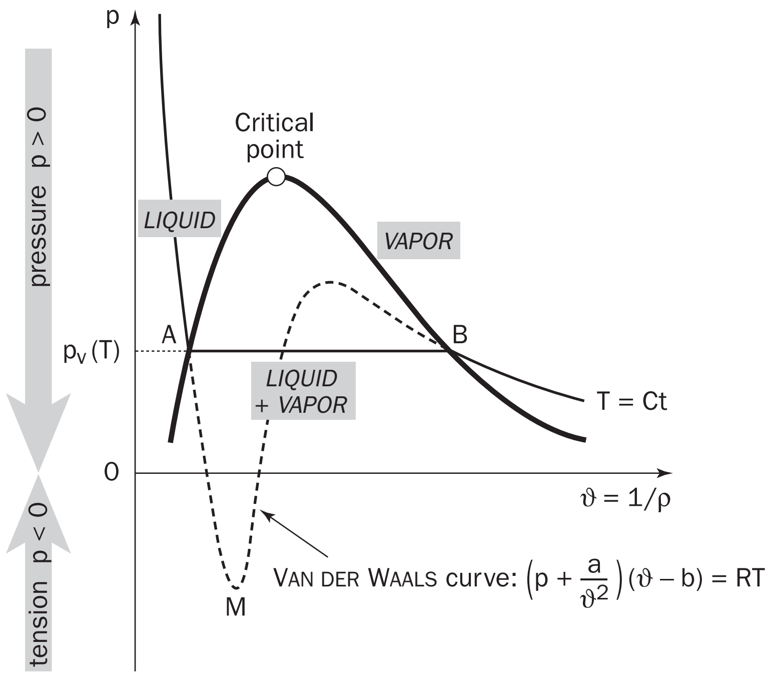

1.2 - **Andrews-isotherms**

Even in almost static conditions, a phase change may occur at a pressure lower than p_v. For example, consider the so-called ANDREWS-isotherms in the $p-\vartheta$ diagram, where $\vartheta = 1/\rho$ is the specific volume and ρ the density (fig. 1.2). Such curves can be approximated in the liquid and vapor domains by the VAN DER WAALS equation of state. The transformation from liquid to vapor along the path AM can be avoided, provided special care is taken in setting up such an experiment. Along this path, the liquid is in metastable equilibrium and even can withstand negative absolute pressures, i.e., tensions, without any phase change.

the RAYLEIGH-PLESSET equation (3.12) can be written as follows:

$$\frac{d}{dt}\left(2\pi\rho \dot{R}^2 R^3\right) = \left[p_v + p_{g0}\left(\frac{R_0}{R}\right)^{3\gamma} - p_\infty(t)\right] 4\pi R^2 \dot{R} - 8\pi S R\dot{R} + 16\pi\mu R\dot{R}^2 \tag{3.14}$$

The term on the left-hand side represents the variation in kinetic energy of the liquid body. The first term on the right-hand side represents pressure forces acting on the liquid, while the surface tension forces are represented by the second term. The dissipation rate due to viscosity is expressed as $\iiint 2\mu\, e_{ij}\, e_{ij}\, d\tau$, where e_{ij} stands for the deformation rate tensor and the integral is taken over the entire liquid volume. This gives the last term.

3.2. *THE COLLAPSE OF A VAPOR BUBBLE*

3.2.1. *ASSUMPTIONS*

In the present section, the effects of viscosity, non-condensable gas and surface tension are all ignored.

Before the initial time, the bubble is supposed to be in equilibrium under pressure $p_{\infty 0}$, which is equal to p_v, according to equation (3.5). From the instant $t = 0$, a constant pressure p_∞, higher than p_v, is applied to the liquid. It results in the collapse of the bubble in a characteristic time τ called the RAYLEIGH time.

This simple model allows us to describe the global features of the first bubble collapse for an almost inviscid liquid such as water. However, it does not provide an account of the successive rebounds and collapses actually observed in various physical situations. It should be noted that, if surface tension were not ignored, the collapse would be only slightly accelerated.

3.2.2. *THE INTERFACE VELOCITY*

With the previous assumptions, the RAYLEIGH-PLESSET equation (3.12) can be integrated using relation (3.13) to give:

$$\rho \dot{R}^2 R^3 = -\frac{2}{3}\left(p_\infty - p_v\right)\left(R^3 - {R_0}^3\right) \tag{3.15}$$

As $\dot{R}$ is negative during collapse, one obtains:

$$\frac{dR}{dt} = -\sqrt{\frac{2}{3}\,\frac{p_\infty - p_v}{\rho}\left[\frac{{R_0}^3}{R^3} - 1\right]} \tag{3.16}$$

The radius tends to 0 and the radial inwards motion accelerates without limit. The numerical integration of this equation allows the calculation of the radius $R(t)$ as a function of time. The characteristic collapse time or RAYLEIGH time is:

$$\tau = \sqrt{\frac{3}{2}\frac{\rho}{p_\infty - p_v}} \int_0^{R_0} \frac{dR}{\sqrt{\frac{R_0^3}{R^3} - 1}} \cong 0.915\, R_0 \sqrt{\frac{\rho}{p_\infty - p_v}} \tag{3.17}$$

The constant 0.915 is the approximate value of $\sqrt{\frac{\pi}{6}}\frac{\Gamma(5/6)}{\Gamma(4/3)}$ where Γ is the factorial gamma function.

3.2
Evolution of R(t) and $\dot{R}(t)$ during bubble collapse

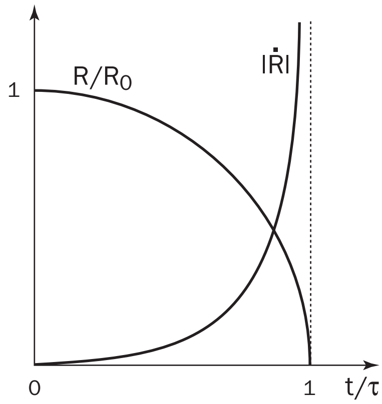

The value of τ is in good agreement with the experimental values for a large range of initial values of the bubble diameter from about one micrometer to one meter. As an example, in the case of water, a bubble with an initial radius of 1 cm collapses in about one millisecond under an external pressure of 1 bar.

The behavior of R(t) and $\dot{R}(t)$ are shown in figure 3.2. While the mean value of the collapse velocity is R_0/τ, $\dot{R}$ tends to infinity at the end of collapse. For R approaching 0, the interface velocity has the following strong singularity:

$$\left|\dot{R}\right| \cong \sqrt{\frac{2}{3}\frac{p_\infty - p_v}{\rho}} \left[\frac{R_0}{R}\right]^{3/2} \cong 0.747\, \frac{R_0}{\tau}\left[\frac{R_0}{R}\right]^{3/2} \tag{3.18}$$

At the end of the collapse, the radius evolves according to the law:

$$\frac{R}{R_0} \cong 1.87 \left[\frac{\tau - t}{\tau}\right]^{2/5} \tag{3.19}$$

With the previous numerical values, it is found that $\left|\dot{R}\right| \approx 720$ m/s for $R/R_0 = 1/20$. Such high values of velocity, of the order of half of the velocity of sound in water, lead us to believe that liquid compressibility must be taken into account in the final stages of collapse.

It must be kept in mind that some other physical aspects, such as the presence of non-condensable gas or the finite rate of vapor condensation, will modify bubble behavior. However, the RAYLEIGH model exhibits the main features of bubble collapse, particularly its short duration and the rapid change in its time scale.

3.2.3. *THE PRESSURE FIELD*

The pressure field $p(r,t)$ can be determined from equation (3.9) in which $\dot{R}$ is known from equation (3.16) and $\ddot{R}$ can be deduced by derivation, which gives:

$$\ddot{R} = -\frac{p_\infty - p_v}{\rho} \frac{R_0^3}{R^4} \tag{3.20}$$

The result of the calculation is:

$$\Pi(r,t) = \frac{p(r,t) - p_\infty}{p_\infty - p_v} = \frac{R}{3r}\left[\frac{R_0^3}{R^3} - 4\right] - \frac{R^4}{3r^4}\left[\frac{R_0^3}{R^3} - 1\right] \tag{3.21}$$

The behavior of non-dimensional pressure Π at several instants is shown in figure 3.3. It exhibits a maximum within the liquid as soon as the bubble radius becomes smaller than $\left(1/\sqrt[3]{4}\right)R_0 \cong 0.63\, R_0$. The maximum pressure is:

$$\Pi_{max} = \frac{p_{max} - p_\infty}{p_\infty - p_v} = \frac{\left[\frac{R_0^3}{4R^3} - 1\right]^{4/3}}{\left[\frac{R_0^3}{R^3} - 1\right]^{1/3}} \tag{3.22}$$

and it occurs at distance r_{max} from the bubble center given by:

$$\frac{r_{max}}{R} = \left[\frac{\frac{R_0^3}{R^3} - 1}{\frac{R_0^3}{4R^3} - 1}\right]^{1/3} \tag{3.23}$$

When R/R_0 becomes small, the two previous relations give approximately:

$$\Pi_{max} \approx \frac{1}{4^{4/3}}\left[\frac{R_0}{R}\right]^3 \cong 0.157\left[\frac{R_0}{R}\right]^3 \tag{3.24}$$

$$\frac{r_{max}}{R} \approx \sqrt[3]{4} \cong 1.59 \tag{3.25}$$

Very high pressures close to the bubble interface are reached. For example, for $R/R_0 = 1/20$, $p_{max} = 1{,}260$ bars if $p_\infty - p_v$ is one bar.

Attention must be paid to the kind of pressure wave that appears in figure 3.3 during the collapse of the bubble. As only pressure and inertia forces are taken into account in the present model, this pressure wave propagating inward must be considered as the effect of inertia forces only. More complicated models exhibit a similar behavior.

From a physical viewpoint, the violent behavior of bubble collapse results from two main facts:

- the pressure inside the bubble is constant and does not offer any resistance to liquid motion;
- the conservation of the liquid volume, through spherical symmetry (eq. 3.6), tends to concentrate liquid motion to a smaller and smaller region.

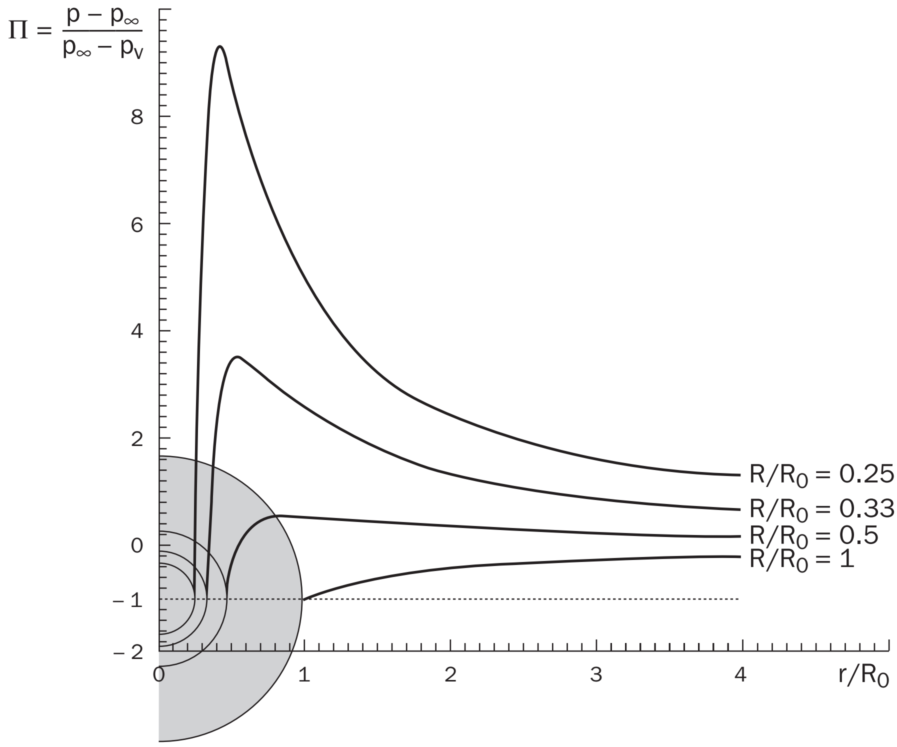

3.3 - Evolution of the pressure field during bubble collapse

3.2.4. *REMARK ON THE EFFECT OF SURFACE TENSION*

If surface tension is taken into account, equation (3.16) becomes:

$$\frac{dR}{dt} = -\sqrt{\frac{2}{3}\frac{p_\infty - p_v}{\rho}\left[\frac{R_0{}^3}{R^3} - 1\right] + \frac{2S}{\rho R_0}\frac{R_0{}^3}{R^3}\left[1 - \frac{R^2}{R_0{}^2}\right]} \tag{3.26}$$

The accelerating effect of surface tension becomes significant if:

$$\frac{2S}{\rho R_0} > \frac{2}{3}\frac{p_\infty - p_v}{\rho} \tag{3.27}$$

i.e.

$$R_0 < \frac{3S}{p_\infty - p_v} \tag{3.28}$$

6. SUPERCAVITATION

As the cavitation parameter is decreased, a small cavity attached to a hydrofoil will extend and grow longer and longer. It becomes a supercavity as soon as it ceases to close on the cavitator wall but inside the liquid, downstream of the cavitator. Simultaneously, the lift of the hydrofoil decreases while its drag increases.

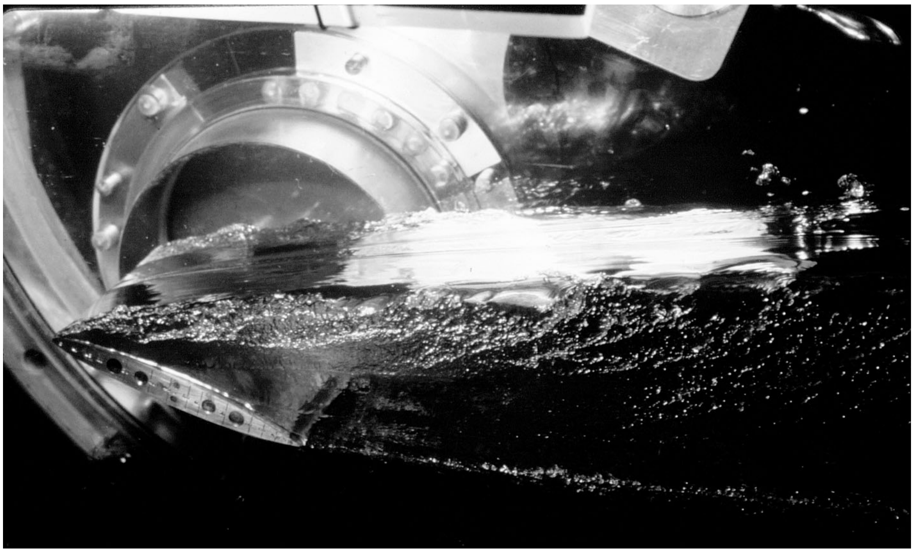

6.1 - Supercavity behind a two-dimensional NACA 16012 hydrofoil
(REYNOLDS number 10^6, cavitation parameter 0.07, angle of attack 17 deg.)

For very high relative velocities between the liquid and the body, it is practically impossible to use non-cavitating foils, such as the conventional ones used in aerodynamics. In such cases, different types of supercavitating foils have been designed for better efficiency, such as truncated foils with a base cavity or supercavitating foils with non-wetted uppersides.

This chapter begins with a presentation of the main physical aspects of supercavities (§ 6.1). Although the background of applications was chosen rather on the side of two-dimensional, lifting bodies, most of the features are applicable to axisymmetric supercavities. After a section devoted to the basis of flow modeling (§ 6.2), some typical results are given in section 6.3. The case of axisymmetric supercavities is considered at the end of the chapter (§ 6.4).

8.1.2. CAVITY PATTERNS ON A TWO-DIMENSIONAL FOIL

In the case of hydrofoils, various cavity flow patterns can be observed according to the angle of attack and the cavitation number. For a proper observation of attached cavities in a hydrodynamic tunnel, it is essential to eliminate as much as possible traveling bubble cavitation in favor of attached cavities, and hence to use strongly deaerated water, so that almost no nucleus is activated.

Figure 8.3 gives a mapping of the various cavity flow patterns which have been observed on a NACA 16012 hydrofoil, for a fixed REYNOLDS number, when the incidence and the cavitation number (or simply the ambient pressure) are modified [FRANC & MICHEL 1985].

For small values of the cavitation number, supercavitation is observed for any angle of attack. The supercavity detaches itself from the rear part of the foil for an angle of attack of around zero (region 1), and the detachment point progressively moves upstream, towards the leading edge, as incidence increases. The detachment line is almost straight in the spanwise direction in regions 1 and 3, whereas it becomes strongly three-dimensional in the intermediate zone 2.

In region 1, the detachment point is far downstream of the point of minimum pressure, which is close to the point of maximum foil thickness. Thus, as for trans-critical flow around a cylinder, the liquid particles are in a metastable state in front of the cavity. This is why deaerated water is needed to observe this cavity flow regime.

For high values of the cavitation number, the pattern progressively evolves from a partial pure vapor cavity (region 3'), to a two-phase cavity (region 4) with a smaller void fraction and, finally, to cavitation in the shear layer bordering the recirculating zone due to stall at high angle of attack (region 5).

Within a very narrow domain of attack angles (around 4 degrees), the behavior of the cavity flow is rather unexpected. When the cavitation number is decreased from non-cavitating conditions, a leading edge cavity appears first. As the cavitation number is further decreased, the leading edge cavity completely disappears before a new cavity develops, at sufficiently low values of the cavitation number. The disappearance of the leading edge cavity is associated with an unexpected displacement of the detachment point, which moves downstream as σ_v decreases until the cavity disappears. This behavior, connected to the S-shaped limiting curve, results from the strong interaction between the cavity and the boundary layer. Similar behavior of the detachment point was also observed by MICHEL (1988) on a different foil, for velocities of up to 30 m/s, and approximately the same σ_v-values.

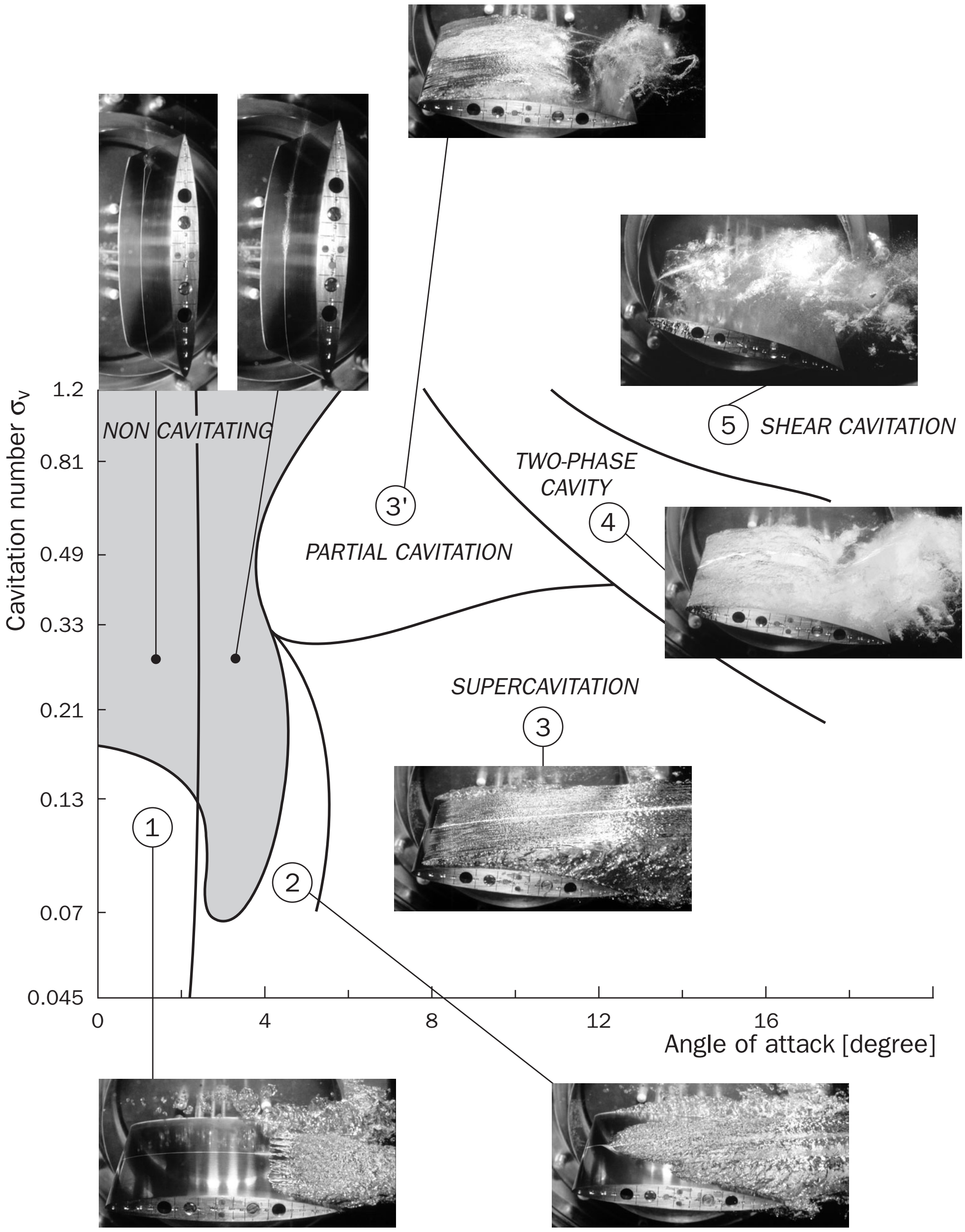

8.3 - Cavity patterns on a NACA 16012 hydrofoil at Re $= 10^6$ in strongly deaerated water

The foil is set at mid-height in the free surface channel of a hydrodynamic tunnel. The foil chord is 0.10 m and the channel height 0.40 m [from FRANC *&* MICHEL*, 1985].*

8.1.2. CAVITY PATTERNS ON A TWO-DIMENSIONAL FOIL

In the case of hydrofoils, various cavity flow patterns can be observed according to the angle of attack and the cavitation number. For a proper observation of attached cavities in a hydrodynamic tunnel, it is essential to eliminate as much as possible traveling bubble cavitation in favor of attached cavities, and hence to use strongly deaerated water, so that almost no nucleus is activated.

Figure 8.3 gives a mapping of the various cavity flow patterns which have been observed on a NACA 16012 hydrofoil, for a fixed REYNOLDS number, when the incidence and the cavitation number (or simply the ambient pressure) are modified [FRANC & MICHEL 1985].

For small values of the cavitation number, supercavitation is observed for any angle of attack. The supercavity detaches itself from the rear part of the foil for an angle of attack of around zero (region 1), and the detachment point progressively moves upstream, towards the leading edge, as incidence increases. The detachment line is almost straight in the spanwise direction in regions 1 and 3, whereas it becomes strongly three-dimensional in the intermediate zone 2.

In region 1, the detachment point is far downstream of the point of minimum pressure, which is close to the point of maximum foil thickness. Thus, as for trans-critical flow around a cylinder, the liquid particles are in a metastable state in front of the cavity. This is why deaerated water is needed to observe this cavity flow regime.

For high values of the cavitation number, the pattern progressively evolves from a partial pure vapor cavity (region 3'), to a two-phase cavity (region 4) with a smaller void fraction and, finally, to cavitation in the shear layer bordering the recirculating zone due to stall at high angle of attack (region 5).

Within a very narrow domain of attack angles (around 4 degrees), the behavior of the cavity flow is rather unexpected. When the cavitation number is decreased from non-cavitating conditions, a leading edge cavity appears first. As the cavitation number is further decreased, the leading edge cavity completely disappears before a new cavity develops, at sufficiently low values of the cavitation number. The disappearance of the leading edge cavity is associated with an unexpected displacement of the detachment point, which moves downstream as σ_v decreases until the cavity disappears. This behavior, connected to the S-shaped limiting curve, results from the strong interaction between the cavity and the boundary layer. Similar behavior of the detachment point was also observed by MICHEL (1988) on a different foil, for velocities of up to 30 m/s, and approximately the same σ_v-values.

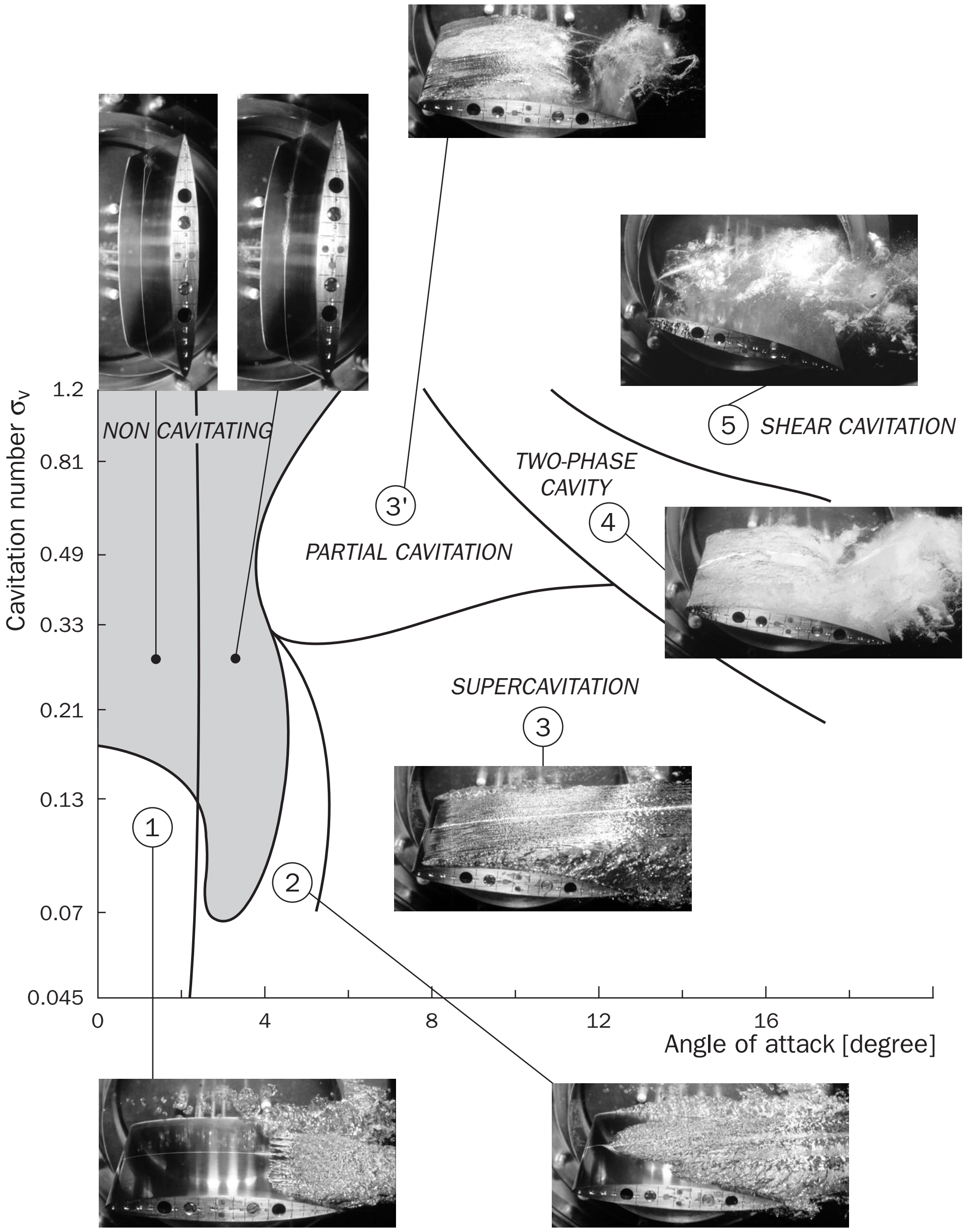

8.3 - Cavity patterns on a NACA 16012 hydrofoil at $Re = 10^6$ in strongly deaerated water

The foil is set at mid-height in the free surface channel of a hydrodynamic tunnel. The foil chord is 0.10 m and the channel height 0.40 m [from FRANC & MICHEL, 1985].

The radial equilibrium equation:

$$\frac{\partial p}{\partial r} = \rho \frac{v_\theta^2}{r} \tag{10.22}$$

allows us to compute the radial pressure distribution and more especially the minimum pressure p_{min} at the vortex center from the pressure at infinity p_∞.

For a RANKINE vortex, the minimum pressure is given by:

$$\frac{p_{min} - p_\infty}{\rho} = -\left[\frac{\Gamma}{2\pi a}\right]^2 \tag{10.23}$$

whereas, for a BURGERS vortex, it is given by:

$$\frac{p_{min} - p_\infty}{\rho} = -0.871\left[\frac{\Gamma}{2\pi a}\right]^2 \tag{10.24}$$

Cavitation occurs on the vortex axis when the minimum pressure falls below the vapor pressure p_v. The velocity and pressure distributions for both models are compared in figure 10.6.

10.2.3. TIP VORTEX STRUCTURE

Tangential velocity

In the past, experimentation has been the only means of obtaining information on the vortex structure. STINEBRING *et al.* (1991) were the first to measure the velocity field at a small distance from the tip, in the case of a trapezoidal lifting surface. They showed that the vortex is fully three-dimensional in the close wake of the wing.

FRUMAN *et al.* (1991, 1992a, 1992b, 1993) and PAUCHET *et al.* (1993) conducted systematic measurements of the axial and tangential components of the velocity at various stations within a short distance downstream of the tip. Figure 10.7 presents the evolution of the tangential velocity profiles along the tip vortex for an elliptical foil. Let us recall that the tip vortex flow is not axisymmetric in the vicinity of the tip and that figure 10.7 gives only a partial idea of the vortex structure.

A central zone with solid body rotation is clearly visible. The rotation rate is very high, larger than 1,000 revolutions per second for the present operating conditions. The maximum velocity first increases rapidly, reaches a maximum at a distance of about 0.125 c_{max} before decreasing slowly.

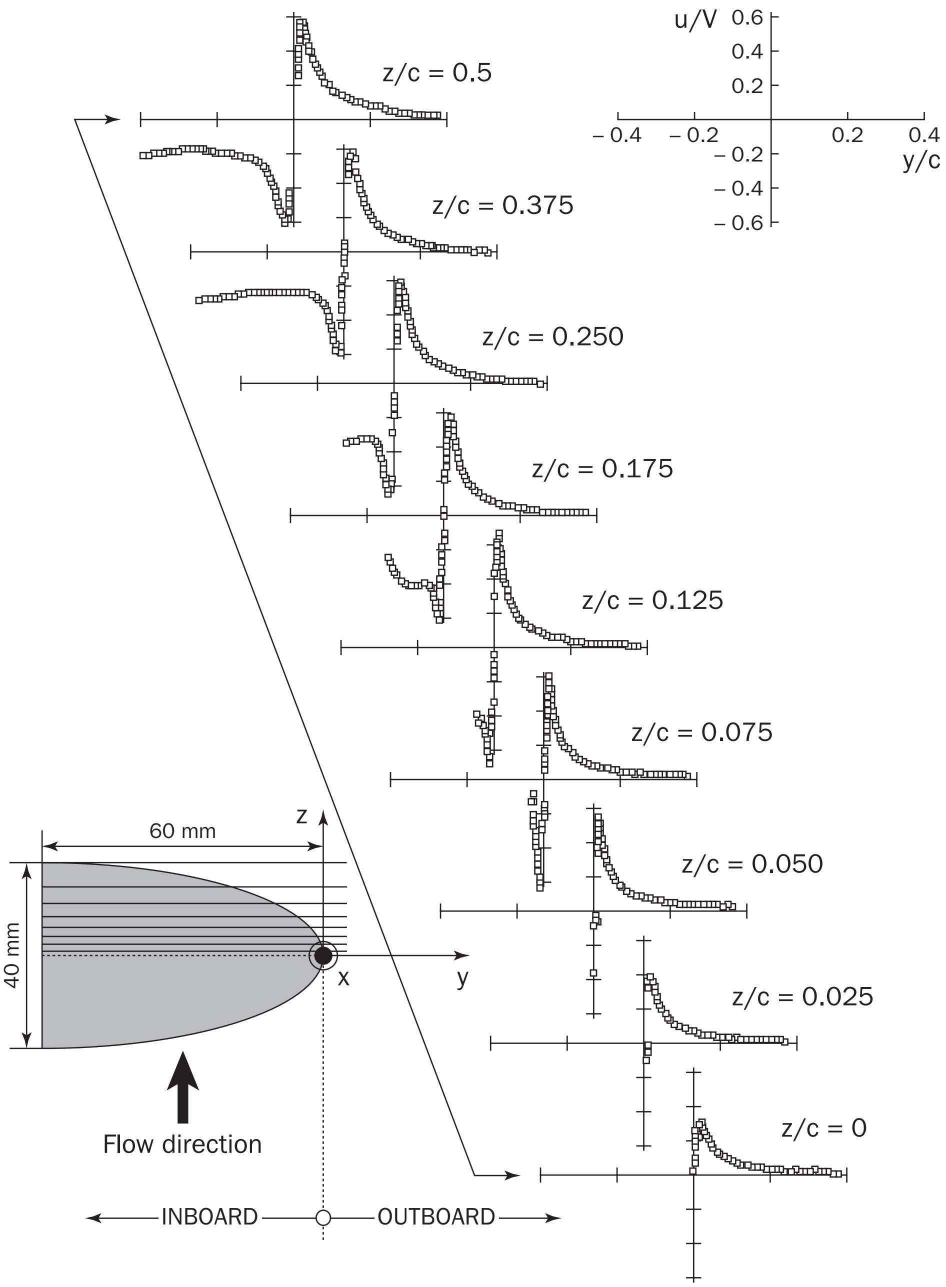

10.7 - Tangential velocity profiles at different stations z along the vortex path

(NACA 16020, maximum chord length at root $c = 40$ mm, $AR = 3.8$, incidence $= 10.6°$ and $V = 9$ m/s)

The component presented here is that along the x-axis. It is non-dimensionalized by the incoming velocity V and plotted as a function of the distance y from the vortex center [from FRUMAN et al., 1992b].